The 2010 IEEE/RSJ International Conference on
Intelligent Robots and Systems
October 18-22, 2010, Taipei, Taiwan

Controlling Redundant Robot Arm-Trunk Systems for Human-like Reaching Motion

Tapomayukh Bhattacharjee, Yonghwan Oh*, Ji-Hun Bae and Sang-Rok Oh

Abstract— **In this paper, we have developed a novel control law to exhibit human-motion characteristics in redundant robot arm-trunk systems for reaching tasks. This newly developed method nullifies the need for the computation of pseudo-inverse of Jacobian while the formulation and optimization of any artificial performance index is not necessary. The time-varying properties of the muscle stiffness and damping as well as the low-pass filter characteristics of human muscles have been modeled by the proposed control law. The newly developed control law uses a time-varying damping shaping matrix and a bijective joint muscle mapping function to describe the human-motion characteristics for reaching motion like quasi-straight line trajectory of the end-effector and symmetric bell shaped velocity profile. The aspect of self-motion and repeatability, which are inherent in human-motion, are also analyzed and successfully modeled using the proposed method. Simulation results show the efficacy of the newly developed algorithm in describing the human-motion characteristics.**

I. INTRODUCTION

Control of redundant humanoid arm systems for reaching motion should achieve human-motion characteristics like quasi-straight line trajectory of human arm and bell-shaped tangential velocity profile for their acceptability in human society. They, however, have a problem of ill-posedness of inverse kinematics. Many control strategies employ an artificial performance index to avoid this problem, which when minimized, can lead to the unique determination of the joint space trajectory corresponding to the end-effector path. Some of those performance indices include minimization of joint jerks [1], torque changes [2],efforts during movements [3], input energy [3], joint torques [4], fatigue functions [5] and manipulability indices [6], etc. However, these performance indices have been based on various hypothesis about generation of human movements without any physiological evidence or principles behind their choice [7], [8]. In addition, most of the above approaches require the cumbersome computation of the pseudo-inverse of Jacobian either directly or indirectly. Arimoto *et. al.*, however, came up with a control algorithm which neither requires any artificial performance index nor does it require the computation of the pseudo-inverse of Jacobian but failed to exhibit necessary human-motion characteristics for reaching tasks [7], [8]. Their algorithm could successfully imitate the quasi-straight line trajectory of the end-effector but failed to mimic the symmetric bell-shaped velocity profile [7], [8]. Their subsequent work claim to have improved the velocity profile by using non-linear time-varying stiffness function [9] but the results are still not satisfactory.

Most of the above studies regarding human reaching movements do not take into consideration the effect of trunk contribution in the arm movement. However, the trunk contribution is a major part for reaching points which are normally out of reach [10]. The focus of this study is to consider human reaching motion involving the trunk for the above cases and to the best of authors' knowledge, this is the first time that efforts have been made to come up with a control law which involves the trunk contribution for human reaching motions. The new control scheme successfully demonstrates both quasi-straight line end-point trajectory and symmetric bell-shaped velocity profile. In addition to the issues of the computation of pseudo-inverse of Jacobian and imitating human-motion spatial characteristics identified above, the reaching movements for arm-trunk systems have some additional temporal constraints. Researchers have concluded that the peak velocity of the trunk should occur after the peak velocity of the arm [11], [12] and the trunk motion precedes the arm motion by around $10\,\text{ms}$ [11] but ends almost $100-200\,\text{ms}$ after the arm motion ends [11]. The control scheme developed in this paper also exhibits these temporal characteristics of arm-trunk motion successfully. In addition, this paper analyzes the aspect of self-motion and repeatability in redundant arm-trunk systems which are inherent characteristics of human reaching motion and are successfully demonstrated by the new control scheme. Real-time simulation results using *RoboticsLab* software show the effectiveness of the proposed scheme.

II. HUMAN MOTION CHARACTERISTICS

Human motion occurs as a result of various muscle movements, their coordination and the brain muscle communication. For reaching or pointing movements, the primary human motion characteristics which have been identified were the quasi-straight line trajectory of the arm and symmetric bell shaped velocity profile as shown in Fig. 1 [10], [11]. However, for reaching movements involving the trunk, additionally researchers have identified some more temporal characteristics such as the peak velocity of the trunk occurs after the peak velocity of the arm which can also be noticed from Fig. 1 [11], [12]. Also, it was noticed that the trunk starts moving with or before the arm by around $10\,\text{ms}$ but

T. Bhattacharjee, Y. Oh, and S. R. Oh are with the Cognitive Robotics Center, KIST, 39-1 Hawolgok-dong, Wolsong Gil 5, Seongbuk-gu, Seoul 136-791, South-Korea {tapo_bhatt, oyh, sroh}@kist.re.kr

J. H. Bae is with the Department of Applied Robot Technology, KITECH, Ansan R&D Center, Sangrok-gu, Ansan 426-791, South-Korea joseph@kitech.re.kr

*Y. Oh is the corresponding author

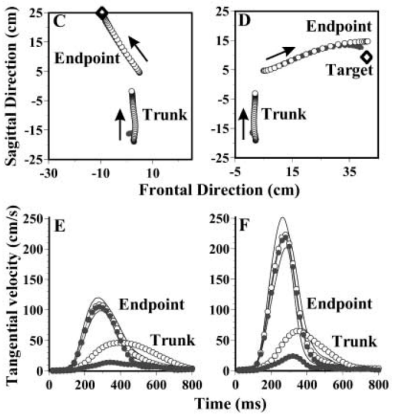

Fig. 1. Characteristics of actual human motion in reaching movements involving the trunk [11].

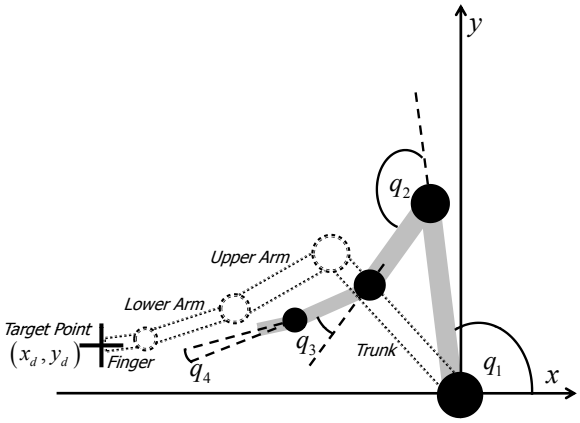

Fig. 2. A 4-DOF robot arm-trunk model.

TABLE I
ROBOT PARAMETERS

	Trunk	Upper Arm	Lower Arm	Index Finger
I_{xx}	0.54	0.0373	0.0285	0.164e-3
I_{yy}	2.30	0.0373	0.0285	0.875e-3
I_{zz}	2.10	9.758e-3	7.370e-3	0.200e-3
ℓ	0.42	0.28	0.28	0.095
m	37	1.407	1.078	0.2423

continues to move even after the arm motion has ceased for around $100 - 200$ ms more [11], [12].

Though there have been many works speculating about the probable causes of such characteristics, there have not been any conclusions and till date the mechanism by which the nervous system controls the redundant degrees-of-freedom to accomplish a task is far from being understood [7]. However, researchers have claimed that human muscles can be modeled using a spring and a damper with time-varying characteristics [13]. It is argued that muscle stiffness drops during movement while muscle damping increases in motion and the variation of these dynamics are in a sinusoidal manner [13], [14]. Also, they are joint-dependent and non-linear in nature [14]. Hence, there is a need for a time-varying, non-linear, joint-dependent model for muscle stiffness and damping. Although, Arimoto *et. al.* have claimed to improve the velocity profile by using a time-varying stiffness model [9], the results were not satisfactory probably because their time-varying model had a sudden and drastic increase in the beginning of the motion and then remained constant thereafter which is unlike the actual behavior noticed [14]. Also, the model in [9] is developed based on an assumption that the actin-myosin interactions which generate the force could be assumed to be a stochastic process and hence, a gamma distribution had been applied. This assumption had no strong evidence. In addition to the above, it has also been identified that human muscles have low-pass filter characteristics and there is a slight delay in brain to muscle communication due to the nervous system path ways which affects the motion pattern [15], [16], [17]. A joint dependent low-pass filter is, therefore, needed to exhibit the low-pass filter characteristics of human muscles. Also, low-pass filters generate an amount of delay which can account for the delay in brain to muscle communication in humans. The proposed control algorithm has been developed based on these needs identified.

III. SYSTEM MODELING

In this paper, we have considered a four degrees of freedom redundant robot in 2-D planar motion for analysis purposes. The four degrees of freedom correspond to the trunk, the upper arm, the lower arm and the index finger. The robot is as shown in Fig. 2 where $q_i,\ (i = 1, \ldots, 4)$ are the generalized coordinates representing the joint angles of the trunk, the upper arm, the lower arm and the index finger respectively. Let I_i denote the inertia tensors for all the links of the robot wherein $i = 1, \ldots, 4$ wherein the diagonal elements are given by $I_{xx},\ I_{yy}$ and I_{zz} which are the principal moments of inertia. The non-diagonal elements given by $I_{xy},\ I_{yz}$ and I_{xz} generally vanish for symmetric construction of the links. Let ℓ_i and m_i denote the link lengths and link masses respectively. The link lengths as well as the dynamic parameters like the link inertia and mass properties are based on normal healthy human data [18], and are given in Table I. All dimensions used in this paper are in S.I units. The upper and lower arms are assumed as cylinders while the index finger is assumed as a cuboid [8].

IV. CONTROL LAW

A new control law has been developed based on the needs identified for characterizing the human motion features in reaching movements involving the trunk. The control law is given below in (1).

$$\boldsymbol{u} = -\boldsymbol{W}_f \Big[\boldsymbol{K}_V \dot{\boldsymbol{q}} + k \boldsymbol{F}_{mus}\, \boldsymbol{J}^T(\boldsymbol{q}) \Delta \boldsymbol{x} \Big], \tag{1}$$

where joint damping matrix $\boldsymbol{K}_V$ is given by

$$\boldsymbol{K}_V = \mathrm{diag}\Big[C_1^*(t) \;\; C_2^*(t) \;\; C_3^*(t) \;\; C_4^*(t) \Big] \tag{2}$$

and

$$C_i^*(t) = C_i \sin\left(\pi \left(\|\Delta \boldsymbol{x}_0\| - \|\Delta \boldsymbol{x}\|\right) / 2 \|\Delta \boldsymbol{x}_0\|\right). \tag{3}$$

k is the virtual spring and $\boldsymbol{F}_{mus}$ is a bijective joint muscle mapping function given by

$$\boldsymbol{F}_{mus} = \text{diag}\begin{bmatrix} f_1^*(t) & f_2^*(t) & f_3^*(t) & f_4^*(t) \end{bmatrix} \tag{4}$$

and

$$f_i^*(t) = f_i \cos\left(\pi \left(\|\Delta \boldsymbol{x}_0\| - \|\Delta \boldsymbol{x}\|\right) / 2 \|\Delta \boldsymbol{x}_0\|\right), \tag{5}$$

where f_i denotes the joint muscle stiffness coefficient and

$$\boldsymbol{W}_f = \text{diag}\left[\frac{1}{\tau_i s + 1}\right], \quad \text{for } i = 1, \ldots, 4\,. \tag{6}$$

As given in the control law shown in (1), the control input to the joint actuators is a function of a damping shaping term given by $\boldsymbol{K}_V$ and a bijective joint muscle mapping function given by $\boldsymbol{F}_{mus}$.

The damping shaping term $\boldsymbol{K}_V$ is assumed to be a diagonal matrix whose elements are time-varying functions. This matrix shapes the control input based on the joint actuator velocities and is taken to be diagonal by assuming, without any loss of generality, that velocity coupling is negligible between the different joints. Each of the diagonal elements is modeled by a sinusoidal function based on the current distance of the end-effector with that of the target point. As shown in (3), $\|\Delta \boldsymbol{x}_0\|$ represents the two-norm of the initial distance of the end-effector with that of the target point while $\|\Delta \boldsymbol{x}\|$ represents the current distance of the end-effector with that of the target point and is updated at every time-instant. The sinusoidal function is so chosen such that the damping shaping term vanishes at the start of the motion as $\|\Delta \boldsymbol{x}\| \rightarrow \|\Delta \boldsymbol{x}_0\|$, and then gradually increases during motion till it reaches a maximum value. This time-varying nature is modeled in accordance with the trend noticed for muscle damping in reaching movements [14]. The weighting factors C_i are tuned for appropriate trajectory and velocity characteristics where $i = 1, \ldots, 4$.

The $\boldsymbol{F}_{mus}$ function on the other hand, is modeled as a time-varying joint dependent bijective muscle mapping function. It is bijective because for every joint actuator there is a unique corresponding one-to-one mapping to a time-varying weighting variable which forms the diagonal elements of the function matrix whose dimension is given by the number of degrees of freedom of the robot. This function, as shown in (4), acts on the virtual work done to reach the target. A virtual spring is attached to the end-effector which literally pulls the robot end-effector towards the target point where k denotes the stiffness of the virtual spring. The spring force generates a virtual work which is required to be done by the joint actuators to move the robot to that desired target position and is given by $k\boldsymbol{J}^T(\boldsymbol{q})\Delta \boldsymbol{x}$. This mechanical work is then mapped to appropriate joint muscle stiffness values by the mapping function given in (4). The time-varying nature of each element is modeled by a cosine function based on the current distance of the end-effector with that of the target point. As shown in (5), the cosine function is so chosen such that the muscle stiffness value is maximum before the motion starts as $\|\Delta \boldsymbol{x}\| \rightarrow \|\Delta \boldsymbol{x}_0\|$, and then gradually decreases during motion. This time-varying nature is modeled in accordance with the trend noticed for muscle stiffness in reaching movements [14].The joint muscle stiffness coefficients f_i are tuned for appropriate trajectory and velocity characteristics where $i = 1, \ldots, 4$.

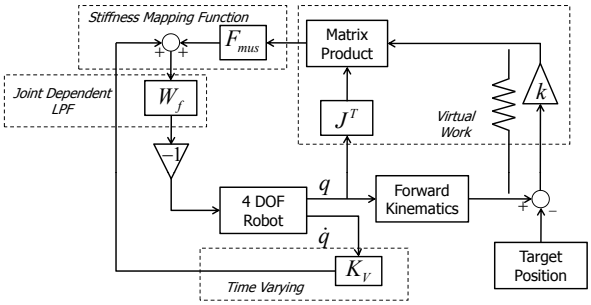

Fig. 3. Block diagram representation of the control law.

This control action is then processed by a low-pass filter matrix, as shown in (6), because muscles exhibit inherent low-pass filter characteristics [15], [16], [17]. The dimension of the matrix corresponds to the number of the degrees of freedom of the robot and each element is modeled as a first-order low pass filter as shown in (6) whose time-constant τ_i is tuned for appropriate behavior. This low-pass filter also introduces a delay between the control input and the joint actuator torque output which functions as the brain-muscle communication delay existing in humans and hence, the time-constant of these joint-dependent filters are important factors in the design of the control law. The resultant control block diagram is shown in Fig. 3.

V. SELF–MOTION AND REPEATABILITY

Self-motion is defined as a combination of joint motions that does not change the end-effector position [19]. It is argued that for human motion, qualitatively, self-motion is never negligible in comparison to the motion component that moves the end-effector. Because at rest the arm is motionless, self-motion increases at the beginning of the movement and decreases at the end of the movement, and is not dependent on the arm configuration or movement speed [19]. The profile of self-motion in actual human reaching motion is shown in Fig. 4. Researchers have argued that self-motion may be the consequence of the trade-off between movement achievement and performance index. Some say that self-motion might arise from a muscle strategy to minimize the energy consumption which eventually reduces the muscle redundancy [19]. However, till date, there is no physiological or neuroanatomical evidence on the existence of any cost function in the Central Nervous System [19]. Additionally, humans are also seen to exhibit repeatability characteristics for closed-loop trajectories and the redundant joints are said to come back almost to their starting positions at the end of the loop [20].

We have taken a natural approach to examine if our control law can exhibit the self-motion and repeatability characteristics of humans in pointing movements. Our control law,

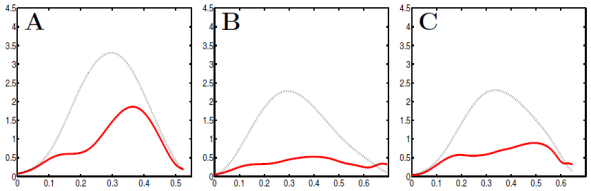

Fig. 4. Self-Motion profile of actual human subjects (A, B and C) in reaching motion [19].

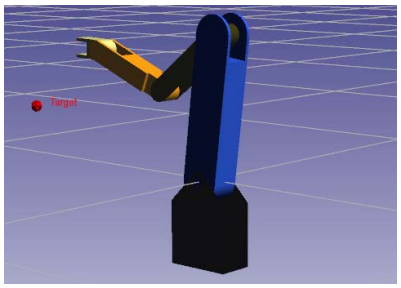

Fig. 5. Model of the robot in *RoboticsLab* real-time simulation software.

which is based on the modeling of the natural behavior of human muscles and muscle-brain communication witnessed through various experiments, tries to achieve the human motion characteristics by virtually adapting the torque input as the work done by human muscles with various stiffness and viscous characteristics. The control parameters are tuned to reach a desired target position with desired trajectory and velocity profile. Then the self-motion profile is plotted to see if the control law, with the tuned parameters, can show similar self-motion profile as that shown in Fig. 4. Also, simulations are conducted to show the repeatability of the robot arm-trunk system under the newly proposed control law for a to-and-fro trajectory between an origin point and a target point, in which our objective is to see if our proposed control law, which takes care of all the necessary human muscle features, can naturally exhibit the inherent repeatability characteristics present in humans.

VI. SIMULATIONS

A four degree-of-freedom robot was, at first, modeled using a CAD software with the same parameters defined in Table I. The robot is as shown in Fig. 5. This model was then imported to a real-time robotic simulation software named *RoboticsLab v1.2.0* as shown in the figure. This real-time simulation software can imitate the experimental conditions coupled with a visual feel of how the robot behaves, which is very important, especially in our cases of simulating human reaching movements. In this simulation, the centers of gravity of the links are calculated based on the actual structure of the robot. The friction and gravity effects are neglected without any loss of generality because, with appropriate friction and gravity compensation techniques, these effects can be nullified which is not the main focus of this paper. Each joint actuator is modeled as a direct drive gearless

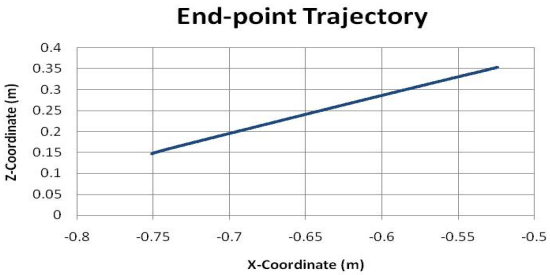

Fig. 6. Quasi-straight line end-point trajectory.

light-weight motor with negligible motor inertia while joint sensors are assumed for position and velocity measurements respectively. The initial conditions of the robot are selected to better visualize the motion and compare it intuitively with that of normal human motion in usual reaching or pointing movements. The initial conditions for this set of simulations are given in (7).

$$\boldsymbol{q}_0 = (83^\circ,\ 135^\circ,\ 300^\circ,\ 20^\circ) \text{ and } \dot{\boldsymbol{q}}_0 = \mathbf{0}. \tag{7}$$

We have selected the target point which can not be reached without moving the trunk and hence trunk has a significant role to play in this reaching task. The corresponding target point coordinates are given in (8).

$$\boldsymbol{p}_d = (x_d,\ y_d) = (-0.75,\ 0.15). \tag{8}$$

The target point is modeled as a sphere by *CustomDraw* function with radius of 0.005 m. The simulation in *RoboticsLab* is updated with 200 Hz frequency. Various simulations were conducted to verify the performance of the proposed control law and to check the self-motion and repeatability characteristics and the results are discussed in details in the next section.

VII. RESULTS AND DISCUSSION

Simulations are done using the real-time robotic simulation software *RoboticsLab* for reaching tasks, which are otherwise out of reach without the involvement of the trunk. Therefore, the trunk involvement in this reaching task is considerably high. The control parameters are tuned to achieve high performance while maintaining the system stability. The damping coefficients C_i are given in (9) while the weighting factors of the muscle stiffness mapping function f_i are given in (10). The virtual spring stiffness is taken to be 0.9.

$$C_1 = 0.75,\ C_2 = 0.03,\ C_3 = 90.5,\ C_4 = 10.970 \tag{9}$$

$$f_1 = 0.28,\ f_2 = 0.78,\ f_3 = 0.6,\ f_4 = 0.4 \tag{10}$$

The time-constants of the joint dependent low-pass filters, as shown in (6), are chosen as in (11).

$$\tau_1 = 1.1,\ \tau_2 = 0.5,\ \tau_3 = 0.8,\ \tau_4 = 0.001. \tag{11}$$

The results of the simulation are shown in Figs. 6 and 7. The redundant robot successfully exhibits quasi-straight line trajectory of the end-effector as shown in Fig. 6, and shows

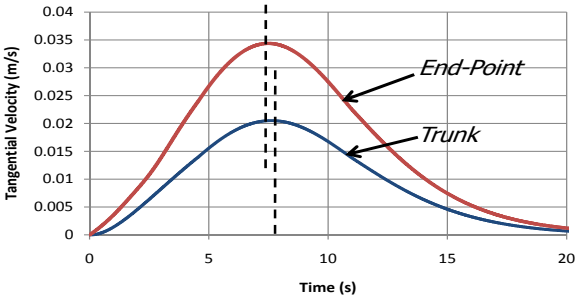

Fig. 7. Comparison of trunk and end-effector velocity profiles.

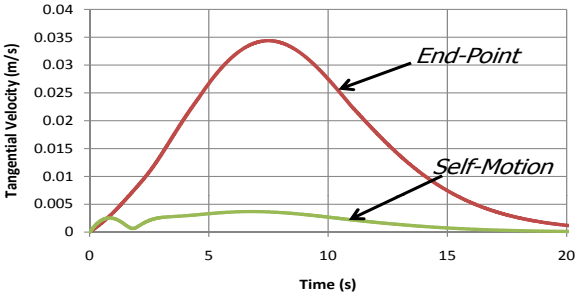

Fig. 8. Comparison of trunk velocity profile and self-motion profile.

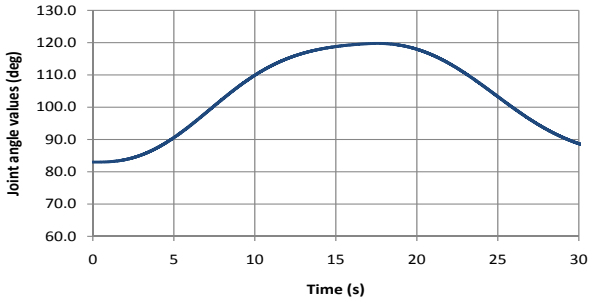

Fig. 9. Trunk joint trajectory.

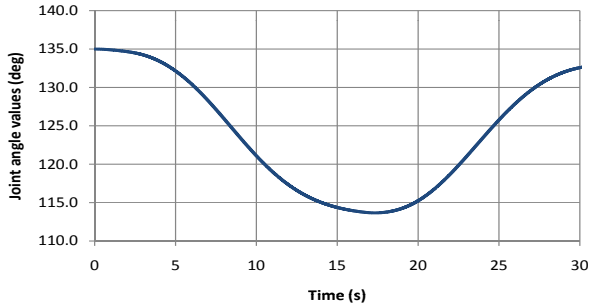

Fig. 10. Shoulder joint trajectory.

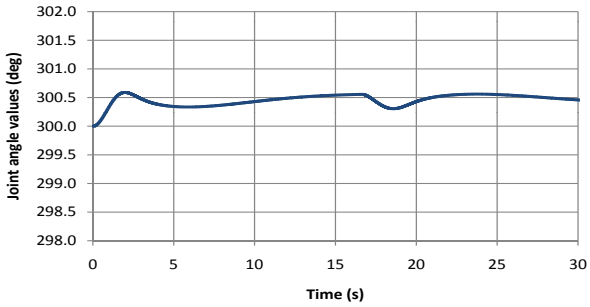

Fig. 11. Elbow joint trajectory.

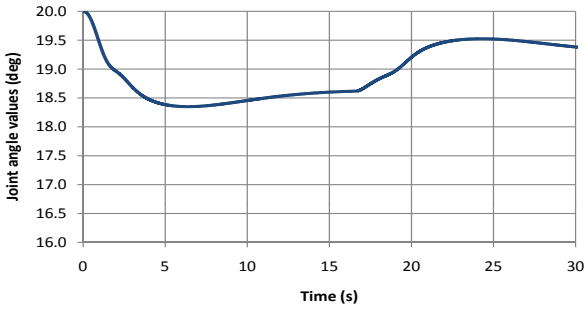

Fig. 12. Index-finger joint trajectory.

symmetric bell-shaped velocity profile of the end-effector as well as the trunk as seen in Fig. 7. The probable reason of the peak velocity of the trunk being lower than that of the end-effector is due to the larger inertia of the trunk joint as compared to the end-effector, which is similar to human motion characteristics. Fig. 7 further proves the efficacy of our algorithm in imitating the temporal characteristics of the human-arm trunk motion. As seen in the figure, the end-effector motion starts almost simultaneously with that of the trunk motion and also ends simultaneously as found in actual experiments [10]. This result is satisfactory considering the fact that the negligible gap of 10 ms during the start of the motion while $100-200$ ms at the end between the trunk and the arm is insignificant in practical cases. Also, it is noted from Fig. 7, that the peak motion of the trunk motion occurs slightly after the peak motion of the end-effector which is also in line with that observed through actual experimental studies involving humans as discussed in Section 2. Thus, the proposed control algorithm can successfully imitate the spatial as well as the temporal characteristics of human arm-trunk motion in reaching movements.

In this paper, we have also tried to simulate the aspect of self-motion and repeatability which are vital human motion characteristics for reaching tasks as discussed earlier in Section V. Self-motion of a robot-manipulator can be analyzed through its null-space velocity basis vectors [19]. The null space velocity basis vectors are found out from the manipulator Jacobian in such a way that the product of the manipulator Jacobian and the null-space basis vectors vanishes [19]. This implies that there is no net motion of the end-effector even though the individual links might move.

A two-norm operation is then performed and the resultant self-motion profile is shown in Fig. 8. It is to be noted with satisfaction that the self-motion profile as given in the figure is similar to the actual human profiles as given in Fig. 4. This shows that our control algorithm can successfully imitate the self-motion characteristics of human reaching motion in addition to the quasi-straight line trajectory of the end-effector and the symmetric bell-shaped velocity profiles of the end-effector and the trunk.

Simulations have also been conducted to check the repeatability of the redundant robot arm-trunk system in which the robot is, at first, made to move from the initial position to the target position after which it is made to return from the target position and trace its path back through the initial position in its movement backward. The joint trajectories of all the four joints of the robot in this single to-and-fro cyclic motion are plotted in Figs. 9, 10, 11, and 12 to check the repeatability. It can be noticed from all these figures that the joint angles come back to their initial configuration quite well, at the end of the motion through the closed-loop trajectory. The trunk joint shows the lowest repeatability with 3.31% while the elbow joint shows the highest repeatability with 0.14%. The shoulder shows 1.61% repeatability while the finger shows a repeatability of 3.35%. Hence, it is quite satisfactory to note that this newly proposed control algorithm shows good repeatability characteristics for all the four joints similar to that of human motion.

VIII. CONCLUSION

In this paper, we have developed a novel control algorithm to exhibit the spatial and temporal characteristics of human reaching movements involving the trunk. This novel control algorithm neither requires the formulation and minimization of any artificial performance index nor involves the cumbersome computation of the pseudo-inverse of the Jacobian. The newly developed control algorithm is developed based on the observed human muscle stiffness and damping properties. This control scheme takes into account the time-varying, joint dependent characteristics of the muscle stiffness and damping as well as the low-pass filter characteristics of human muscles and also considers the communication delay in brain-muscle communication. The aspect of self-motion and repeatability are also analyzed using this novel control law. Simulation results using the real-time robotic simulation software *RoboticsLab* show the efficacy of the algorithm in imitating the spatial as well as temporal characteristics of human arm-trunk motion for reaching tasks. Results also show the effectiveness of this new algorithm in describing the self-motion and repeatability characteristics of the human reaching motion. The average repeatability of all the four joints of the redundant robot arm-trunk system is 2.1% which is very well acceptable considering the human-motion characteristics.

REFERENCES

[1] T. Flash and N. Hogan, "The coordination of arm movements: an experimentally confirmed mathematical model", *Journal of Neuro-Science*, vol. 5, pp. 1688-1703, 1985.

[2] Y. Uno, M. Kawato, and R. Suzuki, "Formation and control of optimal trajectory in human multijoint arm movement", *Biological Cybernetics*, vol. 61, pp. 89-101, 1989.

[3] W. Nelson, "Physical principle for economies of skilled movements", *Biological Cybernetics*, vol. 46, pp. 135-147, 1983.

[4] Z. Hasan, "Optimized movement trajectories and joint stiffness in unperturbed, initially loaded movements", *Biological Cybernetics*, vol. 53, pp. 373-382, 1986.

[5] V. Potkonjak, S. Tzafestas, D. Kostic, G. Djoudjevic, and M. Rasic, "The handwriting problem", *IEEE International Robotics and Automation Magazine*, pp. 35-46, 2003.

[6] T. Yoshikawa, "Manipulability of robotic mechanisms", *International Journal of Robotics Research*, vol. 4, pp. 3-9, 1984.

[7] S. Arimoto, M. Sekimoto, H. Hashiguchi, and R. Ozawa, "Natural resolution of ill-posedness of inverse kinematics for redundant robots: a challenge to Bernstein's degrees-of-freedom problem", *Advanced Robotics*, vol. 19, no. 4, pp. 401-434, 2005.

[8] S. Arimoto, H. Hashiguchi, M. Sekimoto, and R. Ozawa, "Generation of natural motions for redundant multi-joint systems: a differential-geometric approach based upon the principle of least actions", *Journal of Robotic Systems*, vol. 22, no. 11, pp. 583-605, 2005.

[9] S. Arimoto, M. Sekimoto, and R. Ozawa, "A challenge to Bernstein's degrees-of-freedom problem in both cases of human and robotic multi-joint movements", *IEICE Transactions on Fundamentals*, vol. E88-A, no. 10, pp. 2484-2494, 2005.

[10] T. R. Kaminski, C. Bock, and A. M. Gentile, "The coordination between trunk and arm motion during pointing movements", *Experimental Brain Research*, vol. 106, pp. 457-466, 1995.

[11] S. V. Adamovich, P. S. Archambault, M. Ghafouri, M. F. Levin, H. Poizner and A. G. Feldman, "Hand trajectory invariance in reaching movements involving the trunk", *Experimental Brain Research*, vol. 138, pp. 288-303, 2001.

[12] E. Rossi, A. Mitnitski, and A. G. Feldman, "Sequential control signals determine arm and trunk contributions to hand transport during reaching in humans", *Journal of Physiology*, vol. 538, no. 2, pp. 659-671, 2002.

[13] Y. Xu and J. M. Hollerbach, "Identification of human joint Mechanical properties from single trial data", *IEEE Transactions on Biomedical Engineering*, vol. 5, no. 8, pp. 1051-1059, 1998.

[14] D. J. Bennet, J. M. Hollerbach, and I. W. Hunter, "Time-varying stiffness of human elbow joint during cyclic voluntary movement", *Experimental Brain Research*, vol. 88, pp. 433-442, 1992.

[15] D. B. Lockhart and L. H. Ting, "Optimal sensorimotor transformations for balance", *Nature NeuroScience*, vol. 10, no. 10, pp. 1329-1335, 2007.

[16] T. D. J. Welch and L. H. Ting, "A feedback model reproduces muscle activity during human postural responses to support-surface translations", *Journal of Neurophysiology*, vol. 99, pp. 1032-1038, 2008.

[17] J. He, W. S. Levine, and G. E. Loeb, "Feedback gains for correcting small perturbations to standing posture", *IEEE Transactions on Automatic Control*, vol. 38, no. 3, pp. 322-332, 1991.

[18] D. J. Pearsall, J. G. Reid, and R. Ross, "Inertial properties of the human trunk of males determined from magnetic resonance imaging", *Annals of Biomedical Engineering*, vol. 22, pp. 692-706, 1994.

[19] V. Martin, "A dynamical systems account of the uncontrolled manifold and motor equivalence in human pointing movements", *PhD Thesis*, Ruhr-Universiteit, Bochum, Germany.

[20] B. J. W. Waarsing, M. Nuttin, and H. V. Brussel, "Behavior-based mobile manipulation inspired by the human example", in *Proceedings of the IEEE International Conference on Robotics and Automation*, Taipei, Taiwan, pp. 268-273, 2003.